ENVIRONMENTAL RESEARCH
LETTERS

LETTER • OPEN ACCESS

Insights on seasonal solifluction processes in warm permafrost Arctic landscape using a dense monitoring approach across adjacent hillslopes

To cite this article: Sylvain Fiolleau *et al* 2024 *Environ. Res. Lett.* **19** 044021

IOP Publishing Environ. Res. Lett. 19 (2024) 044021 https://doi.org/10.1088/1748-9326/ad28dc

ENVIRONMENTAL RESEARCH
LETTERS

OPEN ACCESS

RECEIVED
30 October 2023

REVISED
26 January 2024

ACCEPTED FOR PUBLICATION
13 February 2024

PUBLISHED
26 March 2024

LETTER

Insights on seasonal solifluction processes in warm permafrost Arctic landscape using a dense monitoring approach across adjacent hillslopes

Sylvain Fiolleau[1,*], Sebastian Uhlemann[1], Ian Shirley[1], Chen Wang[1], Stijn Wielandt[1], Joel Rowland[2] and Baptiste Dafflon[1]

[1] Earth and Environmental Sciences Area, Lawrence Berkeley National Laboratory, Berkeley, CA, United States of America
[2] Division of Earth and Environmental Sciences, Los Alamos National Laboratory, Los Alamos, NM, United States of America
[*] Author to whom any correspondence should be addressed.

E-mail: sfiolleau@lbl.gov

Keywords: Arctic, solifluction, permafrost

Supplementary material for this article is available online

Abstract

Solifluction processes in the Arctic are highly complex, introducing uncertainties in estimating current and future soil carbon storage and fluxes, and assessment of hillslope and infrastructure stability. This study aims to enhance our understanding of triggers and drivers of soil movement of permafrost-affected hillslopes in the Arctic. To achieve this, we established an extensive soil deformation and temperature sensor network, covering 48 locations across multiple hillslopes within a 1 km^2 watershed on the Seward Peninsula, AK. We report depth-resolved measurements down to 1.8 m depth for May to September 2022, a period conducive to soil movement due to deepening thaw layers and frequent rain events. Over this period, surface movements of up to 334 mm were recorded. In general, these movements occur close to the thawing front, and are initiated as thawing reaches depths of 0.4–0.75 m. The largest movements were observed at the top of the south-east facing slope, where soil temperatures are cold (mean annual soil temperatures averaging −1.13 °C) and slopes are steeper than 15°. Our analysis highlights three primary factors influencing movements: slope angle, soil thermal conditions, and thaw depth. The latter two significantly impact the generation of pore water pressures at the thaw–freeze interface. Specifically, soil thermal conditions govern the liquid water content, while thaw depth influences both the height of the water column and, consequently, the pressure at the thawing front. These factors affect soil properties, such as cohesion and internal friction angle, which are crucial determinants of slope stability. This underscores the significance of a precise understanding of subsurface thermal conditions, including spatial and temporal variability in soil temperature and thaw depth, when assessing and predicting slope instabilities. Based on our observations, we developed a factor of safety proxy that consistently falls below the triggering threshold for all probes exhibiting displacements exceeding 50 mm. This study offers novel insights into patterns and triggers of hillslope movements in the Arctic and provides a venue to evaluate their impact on soil redistribution.

1. Introduction

Climate warming induced thawing of permafrost (Lewkowicz and Way 2019, Dobricic *et al* 2020, Smith *et al* 2022), and the increasing frequency of extreme events such as wildfire (Lewkowicz and Harris 2005, Lipovsky *et al* 2006) or major rainfall events (Kokelj *et al* 2015) significantly impact landscape and ecosystem processes (Olefeldt *et al* 2016). Soil movement is a key consequence of permafrost thaw, and poses natural hazards (Patton *et al* 2019, Lader *et al* 2023), causes damage to infrastructure (Darrow *et al* 2016, Hjort *et al* 2022), and influences the carbon budget (Turetsky *et al* 2020, Vascik *et al* 2021). The exact

impact of soil movement on carbon fluxes remains unclear (Pautler *et al* 2010, Lafrenière and Lamoureux 2013, Beamish *et al* 2014, Patton *et al* 2019, Turetsky *et al* 2020). Turetsky *et al* (2020) estimated an approximately 50% uncertainty in calculating the net ecosystem carbon balance when accounting for soil movements, emphasizing the intricate nature of understanding the impact of these processes on carbon emissions.

Solifluction processes in the Arctic encompass slow downslope movements of soil masses due to freeze-thaw processes (Harris *et al* 2011). These processes include frost creep, gelifluction, or plug-like flow (Washburn 1980, Matsuoka 2001). Solifluction is commonly observed in sandy to silty soils having low liquid and plasticity indices (Matsuoka 2001, Harris *et al* 2011), and is often observed during late spring and summer when thaw saturates the soil (Rowley *et al* 2015). Solifluction rates are controlled primarily by slope angle, thaw depth, and water content (Hjort *et al* 2014). It can occur on slopes with angles as low as 1°, although it is more prevalent on slope angles ranging from 5° and 20° (Rowley *et al* 2015). Two-sided freezing, which creates ice lenses near the base of the active layer that acts as a shear zone upon thawing, has been shown to enhance the likelihood of plug-like flow during thawing (Lewkowicz and Clarke 1998).

In non-Arctic environments, extreme precipitation events are commonly recognized as a triggering factor of slope instabilities. However, in Arctic environments, the influence of rainfall is comparatively small (Del Vecchio *et al* 2023), and the ice content of the soil emerges as one of the primary triggering factors for slope instabilities (Mithan *et al* 2021). Thaw consolidation of ice-rich fine-grained soils lead to raised pore water pressures (e.g. Morgenstern and Nixon 1971), where the excess pore-water saturates the weakened thaw layer and reduces the shear strength by lowering the soil's cohesion and internal friction angle (Harris and Lewkowicz 2000, Harris *et al* 2011). Testing of soil-ice specimens showed decreasing shear strength with increasing temperature, with the most significant reduction occurring from −2 to 0 °C (Huang *et al* 2022), which correlates with the temperature range where the strongest change in ice content is often observed (Uhlemann *et al* 2021, Huang *et al* 2022), leading to an increase in unfrozen water content.

Despite recent improvements in the understanding of solifluction processes, field studies investigating the heterogeneity of these processes are still rare, leading to gaps in our understanding of their patterns, the volumes mobilized at small and large scales, and their triggering factors. Particular questions that we aim to answer here are: what are the features (timing, intensity, volumes, and location) and patterns exhibited by solifluction processes throughout the soil thawing season across adjacent hillslopes? What mechanisms act as triggers and what primary factors exert control over these phenomena?

We address these questions by using a novel dense monitoring approach to obtain vertically resolved, continuous observations of soil movement and temperature at tens of locations across multiple adjacent hillslopes throughout the thawing season. This spatially and temporally high-resolution data set enabled us to assess the heterogeneities in soil movement along different slope and permafrost conditions on a watershed scale, and evaluate triggering factors.

2. Site description/material

The study site is situated along the Nome–Teller highway, approximately 65 km northwest of Nome (Mile marker 47), on the western Seward Peninsula in Alaska (figure 1). The approximately 1 km^2 study area includes south, south-east and east facing slopes, separated by two main streams merging towards the bottom of the watershed (figures 1(a) and (c)). The mean slope angle is 13°, ranging from 0 to 42°. The site is predominantly covered by tussock tundra, dwarf shrubs and grasses with some patches of tall shrubs, especially near the streams (Del Vecchio *et al* 2023, figure 1(c)). Bedrock is outcropping at the highest elevations of the south facing slope (figure 1(a)). The geology comprises quaternary deposits and the Precambrian Nome Group, with the presence of metabasalt and impure marble and calc-schist (figure 1(a), Till *et al* 2011). These units are covered by a thin layer of organic material, approximately 0.3–0.5 m thick, overlying silty material of varying thickness (about 2 m in average). Over the past 30 years, the mean annual air temperature has been −6 °C, and has increased by 0.06 °C yr^{-1} (Thornton *et al* 2016, Jafarov *et al* 2018). During the same period, the average rainfall and snowfall were 400 mm yr^{-1} and 300 mm yr^{-1}, respectively (Jafarov *et al* 2018).

The study area is located in a region characterized by discontinuous permafrost. The electrical resistivity tomography (ERT) profiles (figure 1(b), Uhlemann *et al* 2023) illustrate the main subsurface features, including the presence of permafrost, bedrock and taliks (perennially unfrozen layers). The high resistivity values in the high elevations of the south facing profiles indicate the presence of outcropping bedrock that is partially frozen, and permafrost bodies at the lower elevations, indicating permafrost is discontinuous in the watershed. In the remaining profiles, the high resistivity values highlight the presence of frozen bodies separated by taliks (figure 1(b)).

3. Method

3.1. Monitoring

Movement and temperature monitoring were performed using an in-house developed sensor array

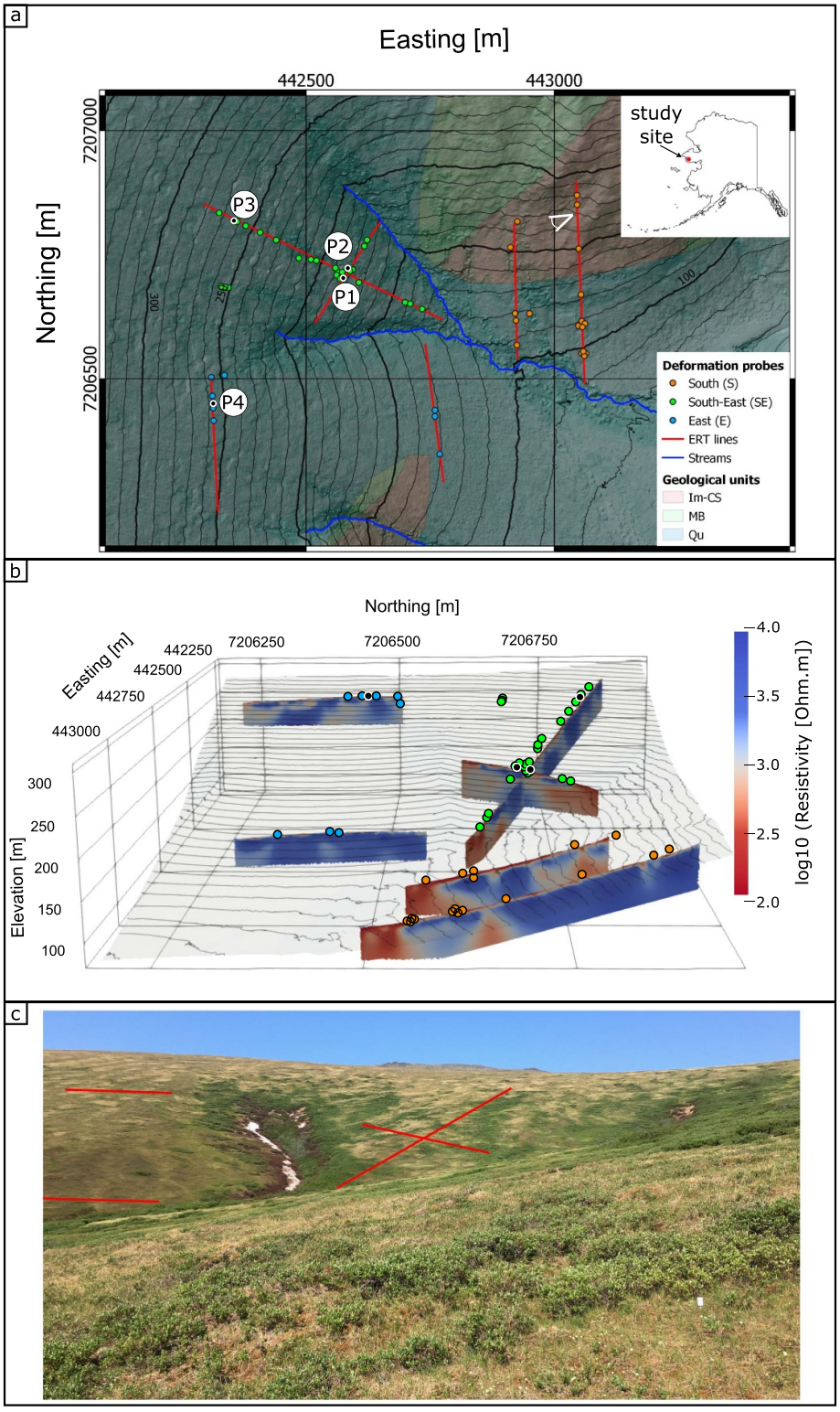

Figure 1. (a) Map of the study site with main streams, ERT profiles and probe locations. Geological units Im-CS, MB and Qu correspond to impure marble and calc-schist of the Nome group, metabasalt of the Nome group and quaternary surficial deposits, respectively (Till *et al* 2011). (b) 3D map of inverted ERT profiles and probe positions across the watershed (Uhlemann *et al* 2023). Colors represent the soil deformation and temperature monitoring locations on south (orange), south-east (green), and east facing (blue) slopes. (c) Photograph of the watershed taken from the South facing slope on 22 June 2022 (view direction indicated by the white icon in (a)).

connected to a low-power consumption data logger (Wielandt *et al* 2022, 2023). A total of 48 probes were installed (figure 1), ranging from 1.2 to 1.8 m in length. Each array consists of three-component MEMS accelerometers (first sensor at 10 cm depth) and temperature sensors, which were placed alternately at 5 cm intervals (Wielandt *et al* 2022, Fiolleau *et al* 2023).

Data collection spanned from 15 September 2021 to 15 September 2022 at 30 min interval. The temperature sensors factory-assured accuracy of 0.1 °C has been verified through lab experiments (Dafflon *et al* 2022). To further increase the accuracy of the temperature data, we applied a constant temperature correction for each sensor by extracting and removing the zero-curtain temperature value, observed during the freezing process during Fall 2022. The movement analysis was focused on the thawing season, specifically from 15 May to 15 September 2022. Before that period pressure build-up at the sensors caused artificially high readings that had to be removed. Among the 48 probes installed, 19 were not anchored into a frozen soil at the end of the monitoring period, however permafrost could still be present deeper than the length of the probes.

The roll, pitch, and yaw angles of each accelerometer are extracted from the accelerometric measurements, allowing the determination of the total angle, which we define as the angle between the vector defined by sensor reading and the gravitational field pointing downwards, without considering the orientation. The movement is calculated from the total angle considering the 10 cm interval between each accelerometer, achieving an accuracy of ± 0.73 mm m^{-1} (Wielandt *et al* 2022). The movement extracted at each sensor corresponds to the temporal cumulative movement from the bottom of the probe to the sensor, considering the deepest sensor as the reference point (0 cm of displacement). The daily velocity at each sensor is determined from the daily gradient of these calculated displacements. To distinctly capture the variations in deformation both over time and along the probe's spatial axis, we also compute the daily gradient of the total angle measured by each sensor throughout the monitoring period. Fluxes are computed using the cumulative displacement (from bottom to the surface) of all sensors for the entire monitoring period.

Additional datasets used to investigate the mechanisms and controlling factors of soil movements include topographic data, weather forcing, and soil moisture measurements. A digital elevation model (DEM) with a spatial resolution of 1 m was derived from LiDAR data acquired in August 2021 by the National Center for Airborne Laser Mapping (Singhania 2020). Rainfall data was obtained from a meteorological station located 30 km south (Nome–Teller highway, mile marker 27, Busey *et al* 2017). Soil moisture content at each probe location was determined using a time domain reflectometry (TDR) meter (Fieldscout TDR150 Soil Moisture Meter) by averaging three measurements performed at 15 cm depth in mid-June 2022. The factory-assured accuracy for volumetric water content is ±3.0%, accompanied by a resolution of 0.1%. The location of each probe was measured using a real-time kinematic global positioning system (RTK differential GPS) with an estimated accuracy of ±2 cm on 20 June 2022 and 14 September 2022.

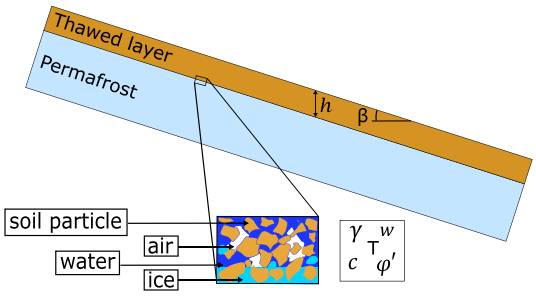

Figure 2. Schematic of parameters impacting slope stability. T is the temperature, β is the slope angle, h the thaw depth, γ the unit weight, w the water content, c the cohesion and φ' the internal friction angle.

3.2. Slope stability analysis

Slope stability refers to the resistance of inclined surfaces against sliding due to external forces. Its assessment involves calculating the balance between the resisting forces that hold the slope in place, i.e. the shear strength, and the driving forces that attempt to make it move. The Mohr–Coulomb failure criterion (Jaeger *et al* 2009) is widely used (Harris and Lewkowicz 2000, Harris *et al* 2008, Bommer *et al* 2012, Wang *et al* 2022) to assess the soil shear strength by considering soil cohesion (soil's internal strength, c in Pa), the internal friction angle (angle threshold before particle starts sliding, φ' in °) and, the pore pressure (u in Pa). The Factor of safety (F_s) is commonly used to assess the ratio of the resisting forces to the driving forces (Nater *et al* 2008, Bommer *et al* 2012):

$$F_s = \frac{c + \left(\gamma h \cos^2\beta - u\right)\tan\varphi'}{\gamma h \cos\beta \sin\beta}. \quad (1)$$

With γ the unit weight (kN m^{-3}), h the thaw depth (m) and β the slope angle (°) (figure 2).

In permafrost environments, McRoberts and Morgenstern (1974) calculated u following:

$$u = \gamma_w h \cos^2\beta + \frac{\gamma' h \cos^2\beta}{1 + \frac{1}{2R^2}} \quad (2)$$

$$\text{With}\,\gamma' = \frac{ds\gamma_w(1+w)}{\gamma} - \gamma_w. \quad (3)$$

With γ_w the water unit weight (kN m^{-3}), R the thaw-consolidation ratio, ds the soil particle density (g cm^{-3}) and w the water content (m^3 m^{-3}), with γ' corresponding to the submerged unit weight.

In alpine permafrost environments, Nater *et al* (2008) calculated c and φ' following:

$$c = -\frac{c_u w_i^{1.91}}{2.1} T \quad (4)$$

$$\varphi' = \varphi'_u - \varphi'_u w_i^{2.6} \quad (5)$$

Table 1. Soil properties used for the computation of the factor of safety (F_s).

Parameters	Values	References
Unfrozen soil cohesion, c_u (kPa)	1	(Hampton and Winters 1983)
Unfrozen soil internal friction angle, $\varphi_u{}'$ (°)	42	(Hampton and Winters 1983)
Unit weight, γ (kN m^{-3})	17	(Lathrop *et al* 2021)
Thaw-consolidation ratio, R	0.15	(Bommer *et al* 2012)
Soil particle density, ds (kN m^{-3})	2.6	(Hampton and Winters 1983)
Water unit weight, γ_w (kN m^{-3})	10	
a	−0.2	(Nater *et al* 2008)
b	0.5	(Nater *et al* 2008)

with w_i the ice content (m^3 m^{-3}), T the soil temperature (°C), c_u the cohesion at a reference temperature (Pa), and φ'_u the internal friction angle for dry soil (°). Nater *et al* (2008) estimated the temperature-dependence (<0 °C) of the ice content w_i with:

$$w_i = a\,T^b \tag{6}$$

where a and b are empirical constants.

In this study, we assess slope failure susceptibility using equations (1)–(6) to calculate F_s and name it F_s proxy. This F_s proxy implies several simplifications and limitations associated with the limited datasets we have and the still limited understanding on the evolution of soil mechanical properties associated with ice-water phase change and thus on the representation of processes leading to soil instability (Fu *et al* 2021). In particular, our F_s proxy is aimed at assessing the susceptibility to failure at annual scale by considering the annual average state of soil and notably the ice content and thaw depth. Thus, for each probe, we define T as the annual mean temperature at 1 m depth (MAT1), h as the maximum thaw depth observed at each location (on 15 September 2022), w based on the TDR measurements by assuming homogeneous conditions throughout the unfrozen layer and thawing season, and β using the slope angle derived from the DEM (at 10 m scale). The other parameters were chosen within the range reported in the literature for unfrozen silty soils (Hampton and Winters 1983, Bommer *et al* 2012) and from nearby soil tests (Lathrop *et al* 2021) (table 1).

A comprehensive sensitivity analysis of our *Fs* proxy was conducted by investigating the influence of the four main parameters (soil water content, MAT1, slope angle, maximum thaw depth) using the Sobol indices and SALib (Herman and Usher 2017, Iwanaga *et al* 2022). The Sobol method, also known as analysis of variance, characterizes the total variance of the model by summing up the variances of the individual inputs (Sobol 2001). This approach allowed us to assess the impact of each input on the model's outcome while excluding interactions with other parameters, focusing solely on the first-order indices.

4. Results

4.1. Movements across the watershed

During the thawing season (May–September) in 2022, observed soil movements were large in places, with local depth-integrated fluxes reaching 0.23 m^2 yr^{-1}, but highly variable (figure 3). The largest soil movements were located high on the south-east facing slope, where MAT1 is lower (minimum −3.22 °C, average −1.13 °C) than further down the slope (maximum 0.76 °C, average −0.62 °C) where there was minimal soil movement. The temperature is the highest in south facing slope (average MAT1 = −0.71 °C), and the most stable. Very small movements were observed at the bottom of this slope where permafrost is still present. The temperature is the lowest in east facing slope (average MAT1 = −1.50 °C). Some soil movements were observed at the top of this slope, although rates were smaller than at the top of the south-east facing slope. No soil movements were observed at the bottom of this slope, which is characterized by small slope angles (<14°) and thin active layer (ERT, figure 1).

4.2. Depth-resolved sliding dynamics and their triggers

Here we explore the mechanisms driving soil movement in the watershed using observed rainfall, soil temperature, displacement, velocity, and total angle gradient (figure 4). We first focus on four probes located on the south-east (P1, P2, P3) and east facing slopes (P4), as depicted in figure 1(a), which are representative of the diverse range of behaviors and soil settings observed across the site. P1 and P2 are situated in the middle of the slope, where the presence of taliks is more pronounced, with resistivities below 3000 Ωm (figure 1(b)). P1 is embedded within a frozen body, while P2, located only 20 m away, is installed in a depression where a talik is present below the seasonally frozen layer. The movements at the surface measured for P1 and P2 were 70 mm and 24 mm, respectively, with fluxes of 0.06 m^2 yr^{-1} and 0.02 m^2 yr^{-1}, respectively. Upon reaching a thaw depth of 1.6 m in mid-July, P2 ceased to be anchored in the frozen layer (figure 4), displaying

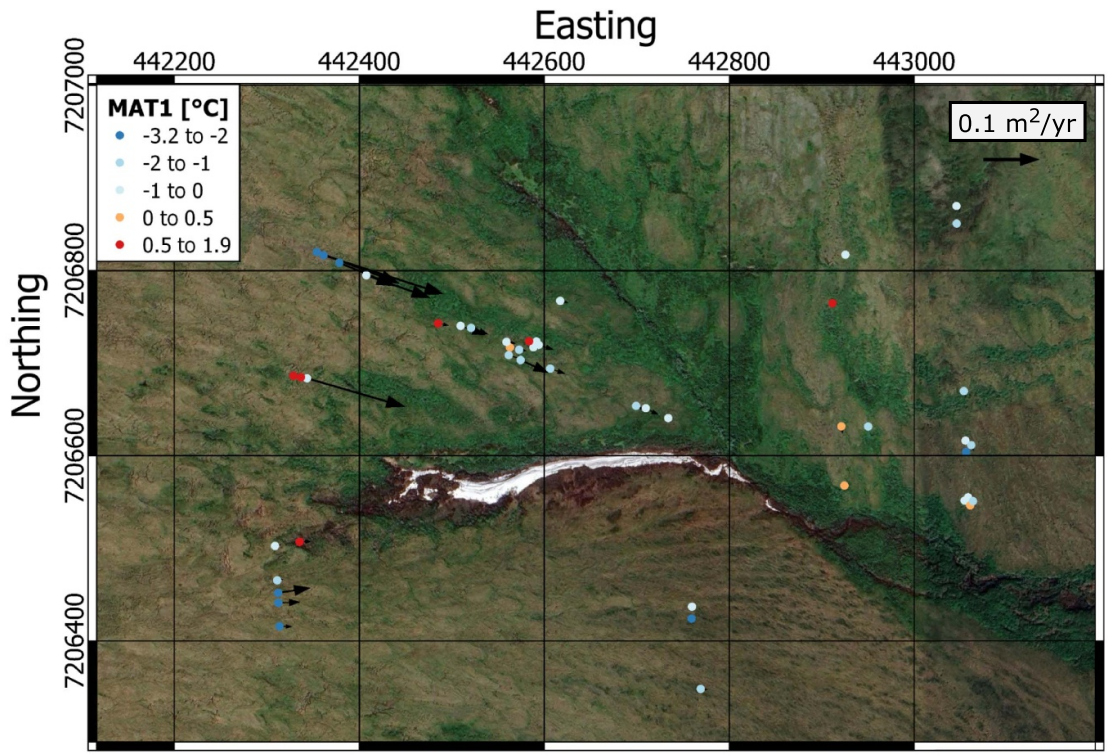

Figure 3. Map showing the fluxes $m^2\ yr^{-1}$ for each probe location and associated MAT1.

increased velocity after rain events on 18 July and 7 August. Movements at location P1 are triggered 4 days before the first rain event in June (see the gradient, figure 4(a)), and experience a clear acceleration following the rain event on 18 July. P3 and P4 are located at the top of the watershed, where colder soil conditions and a thinner active layer prevail (maximum thawing depth of 0.8 and 0.7 m, respectively). The surface displacements measured for P3 and P4 were 334 mm and 119 mm, respectively, with fluxes of 0.23 $m^2\ yr^{-1}$ and 0.06 $m^2\ yr^{-1}$, respectively.

The gradient of the total angle indicates the location and the timing of movements. Its analysis reveals that movement occurs predominantly along the thawing front (figure 4). Across the watershed, soil movement begins after the thawing front has reached depths of 0.4–0.75 m (figures 6 and 7). A shear zone is formed in locations with movement greater than 50 mm (figure 7(b)). In these cases, the shear surface is located at depths ranging between 0.4 and 1.1 m and deepens by an average of about 30 cm during the thawing season (figure 7(b)). Two-sided freezing is observed at locations with large soil movements (e.g. P1, P3, and P4; figure 5), as evidenced by the upward slope in the zero-degree isotherm at depth. This phenomenon, which generates upward freezing, facilitates the formation of ice lenses at the permafrost table, which can contribute to the development of a shear zone upon thawing (Matsuoka 2001).

The spatio-temporal variability in thawing (figure 6(b)) is a strong driver of heterogeneity in movements across the watershed. The east facing slope, characterized by colder permafrost, thaws more slowly (indicated by green to yellow colors at shallow depth in figure 6(b)) than the south facing slope. The south-east facing slope thaws both slowly and quickly at different locations. Soil movements are triggered late in the thaw season on the east facing slope where thawing is slow (August, figure 6(c)), and are slightly smaller than the movements triggered earlier on the south-east facing slope (June–July, figure 6(c)). The south facing slope does not exhibit significant movements even with a rapid thawing process.

Rain events (red dashed lines in figure 6(c)) do not seem to impact soil movement at the top of the watershed, where velocities are large and relatively constant. At some locations where soil movement is otherwise limited (e.g. P2), these rain events are associated with transient spikes, but not long-term increases, in velocity. Almost all of the 19 probes not anchored in the frozen layer exhibited very small displacements (16 mm on average), indicating that locations with a deep active layer or no permafrost are largely stable. However, GPS measurements reveal an additional 5–10 cm of soil movement at six of these probe locations. At these locations, and elsewhere across the watershed, shear zones may be formed deeper than can be sensed by the probes.

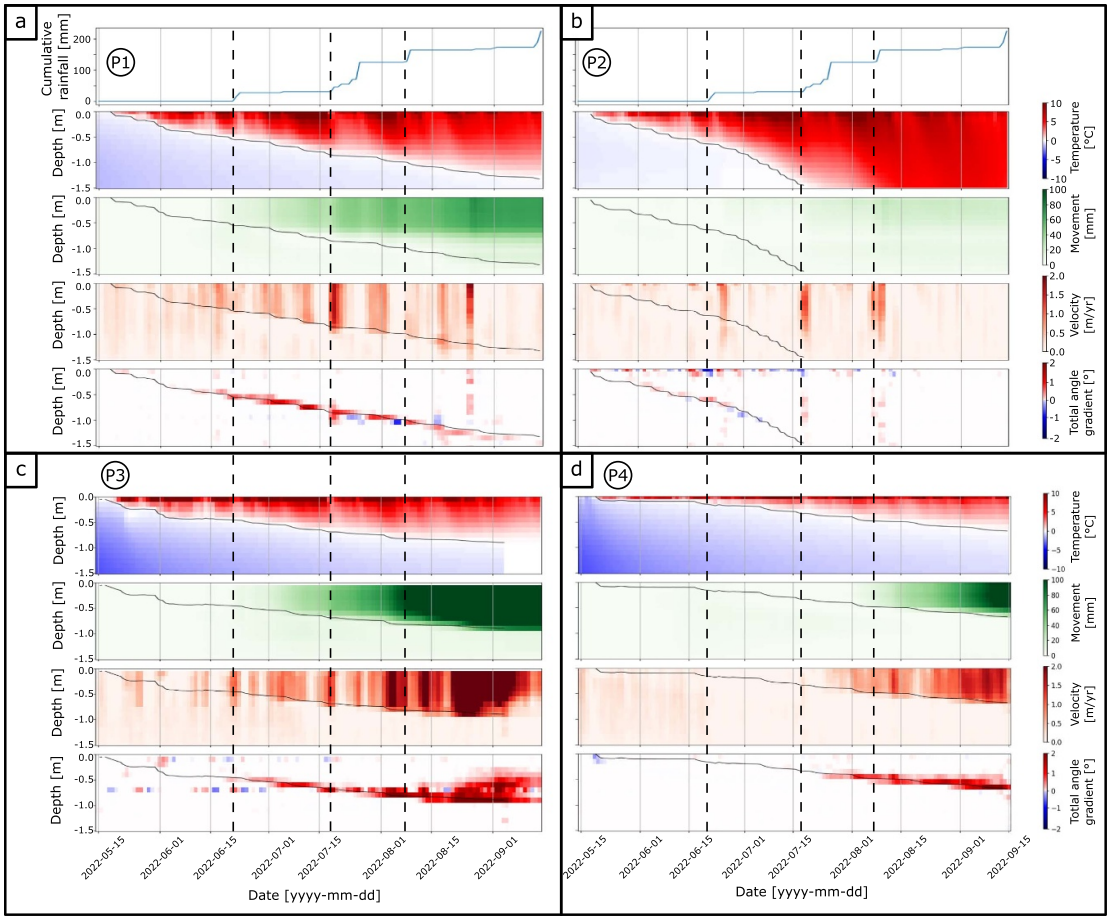

Figure 4. Monitoring data from 15 May to 15 September 2022 at four locations (figure 1). Cumulative rainfall (mm) (a), (b), temperature (°C), movement (mm), velocity (m yr^{-1}), and the gradient of the total angle (°) for each location (a), (b), (c), (d). Dashed vertical lines highlight the main rainfall events, solid black lines show the thaw layer depth defined by the zero-degree isoline.

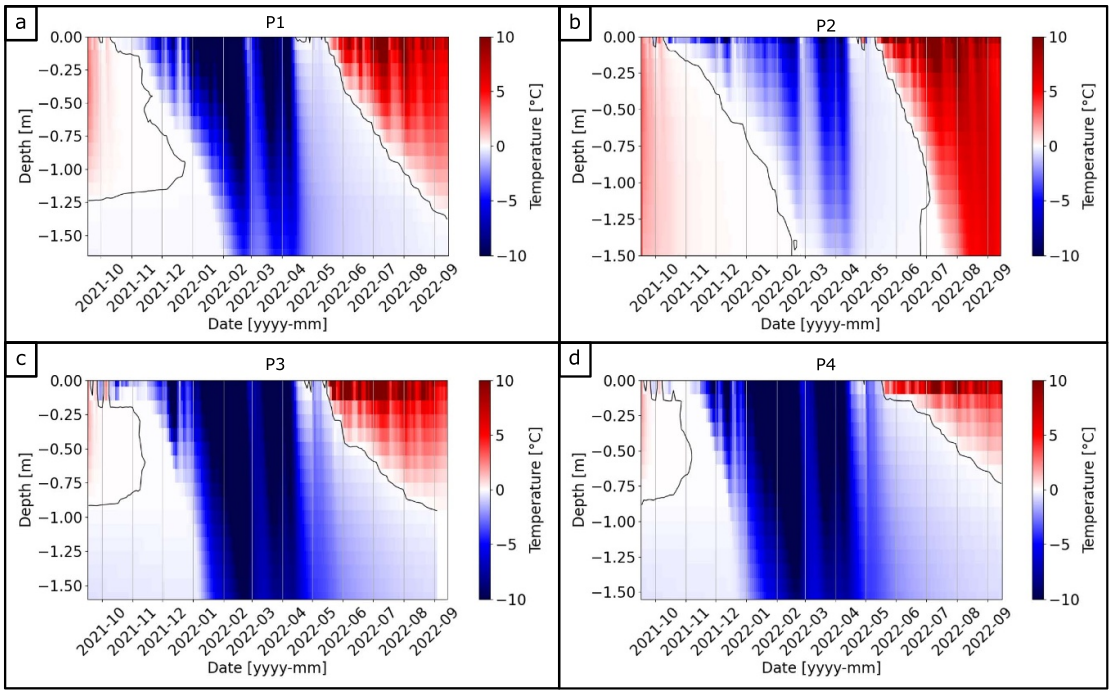

Figure 5. Temperature data from 15 September 2021 to 15 September 2022 for the four locations: P1 (a), P2 (b), P3 (c) and P4 (d). Dashed lines correspond to the zero-degree isoline.

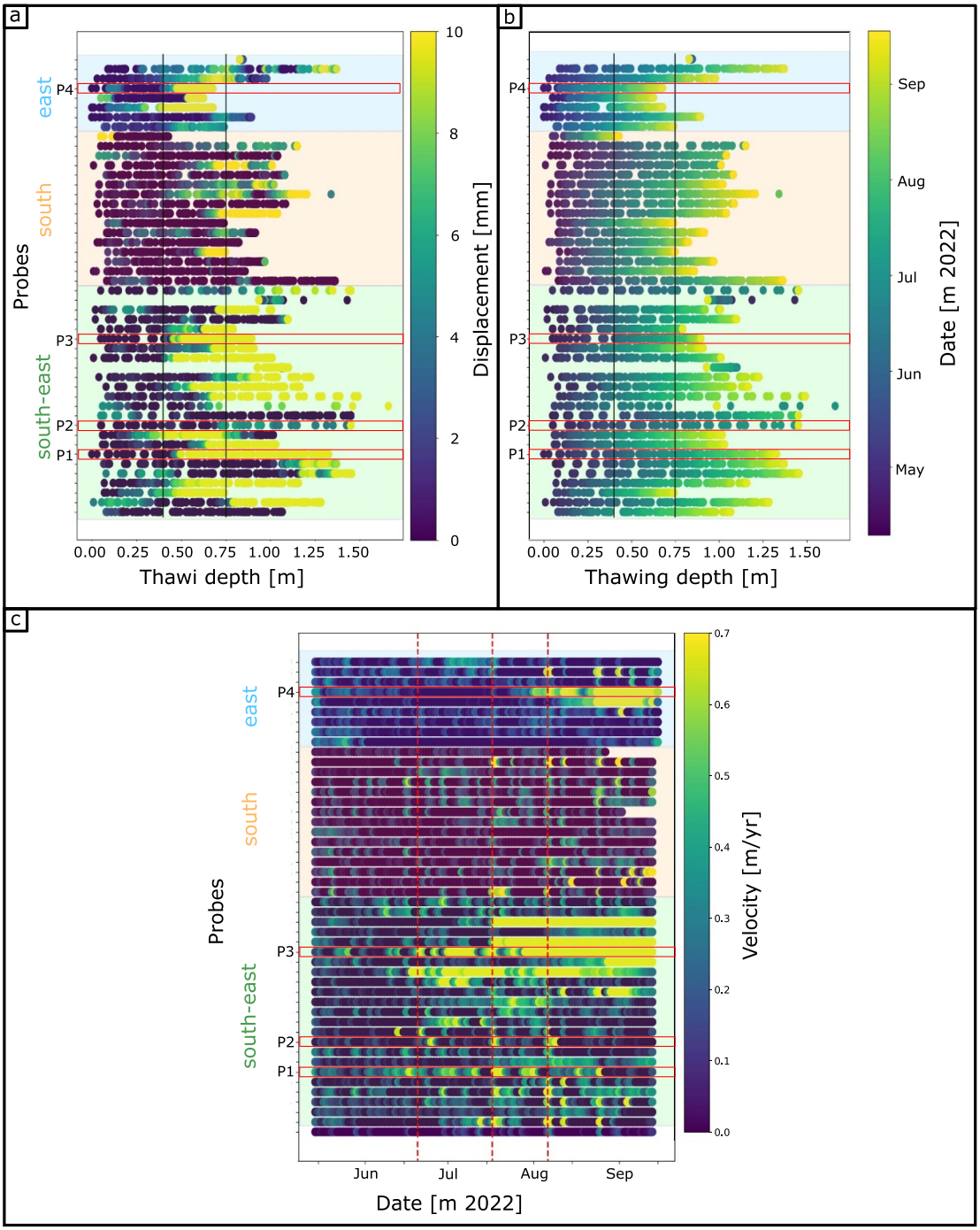

Figure 6. Deformation characteristics of all 48 probes. (a) movement at the surface as function of thawing depth. Black lines highlight 0.4 and 0.75 m thawing depths. (b) Timing of the thawing front depth. (c) Velocity at the surface as function of time. Red dashed lines highlight the main rainfall events (figure 3).

4.3. Controlling factors on slope stability

To assess the potential drivers of solifluction processes, we investigate the relationship between surface displacements and MAT1, slope angle, maximum thawing depth, and moisture content. We focus on 29 probes that are embedded in frozen soil at the end of the monitoring period (figure 8). We find that soil movements larger than 50 mm are only triggered when the slope angle is greater than 15.5°, the moisture content is greater than 33%, MAT1 is below −0.94 °C, and the maximum thaw depth is between 0.65 and 1.3 m (figure 8).

To provide a quantitative measure of the impact of the various soil parameters on soil stability, we perform a sensitivity analysis of the *Fs* proxy (equation (1)). The slope angle has the largest

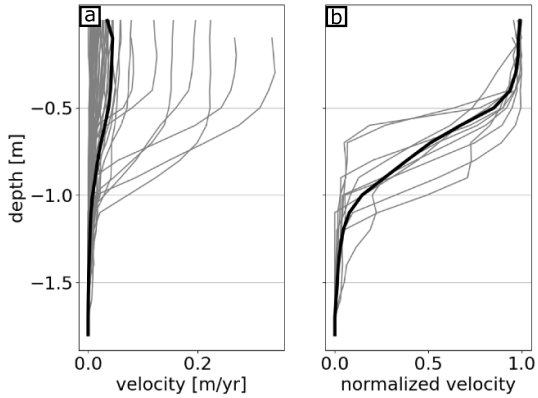

Figure 7. (a) Velocity profiles for the entire monitoring period. Thick black line corresponds to the average value. (b) Normalized velocity profiles for all probes exhibiting more than 50 mm of displacement during the monitoring period. Thick black line corresponds to the average value.

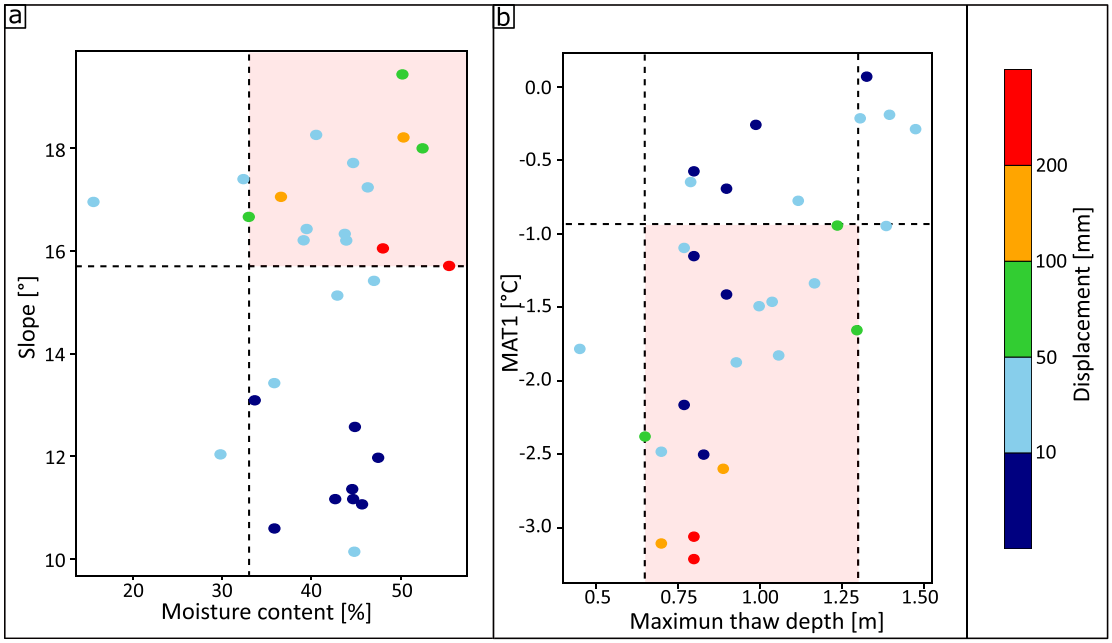

Figure 8. Cross-plots of main parameters controlling the movements of the 29 probes embedded in frozen soil with their associated total surface displacement. (a) Cross plot of slope angle and moisture content. (b) Cross plot of MAT1 and maximum thaw depth. Dotted lines indicate thresholds in main parameters needed to trigger soil movement, red shadow box indicates area where movements could be expected.

influence, followed by MAT1 and maximum thaw depth (figure 9(a)). We evaluated the impact of MAT1 and slope angle on *Fs* by calculating *Fs* using equation (1). Soil moisture was set at an average value of 40%. Subsequently, measurements taken at the 29 locations, where probes were anchored in frozen soil year-round, were integrated for comparison. Below 0 °C, both MAT1 and slope angle fluctuations jointly influence *Fs* (figure 9(b)). As MAT1 decreases, critical *Fs* values (<1) are attained at progressively smaller slope angles. Above 0 °C, the slope angle becomes the main controlling factor. Figure 9(b) also emphasizes that among the 29 locations considered, those with displacements exceeding 50 mm at the surface have an *Fs* below 1 (figure 9(b) and supplementary 1).

5. Discussion

A key finding of this study is that shallow movements within this watershed occur along well-defined shear zones that develop with the thickening of the thaw layer (figure 7(b)), characteristic of plug-like flow (Lewkowicz and Clarke 1998, Del Vecchio *et al* 2023). We find that the initiation of soil movement is linked to the progression of the thaw front, aligning with the conclusion of Harris *et al* (2011), who demonstrated that a specific depth of thawing is required for solifluction movement to occur. Increasing water content near the thaw-freeze interface likely drives a reduction in cohesion and an increase of the internal friction angle (figure 10). Soil movement is triggered if

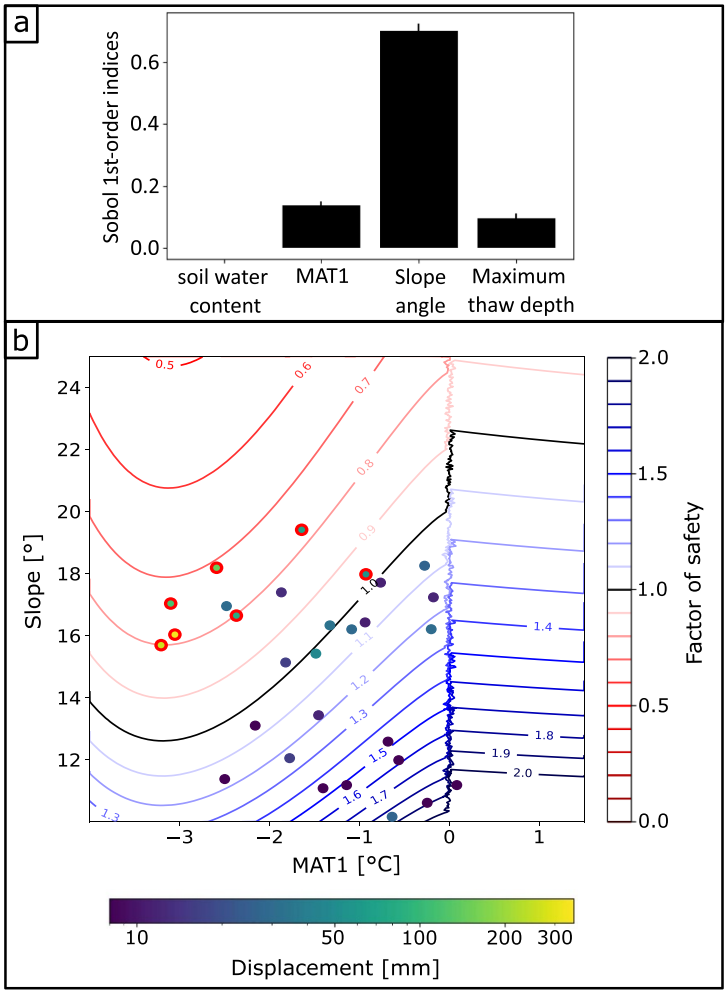

Figure 9. (a) Sensitivity analysis of the four main parameters used in this study in the calculation of the factor of safety, including soil water content, MAT1, slope angle and maximum thaw depth. (b) Isolines showing the variation of the factor of safety in relation to slope angle and temperature fluctuations. Additionally, the 29 locations where probes were embedded in permafrost are represented with their associated surface displacement as color. Probes experiencing displacement greater than 50 mm are circled in red.

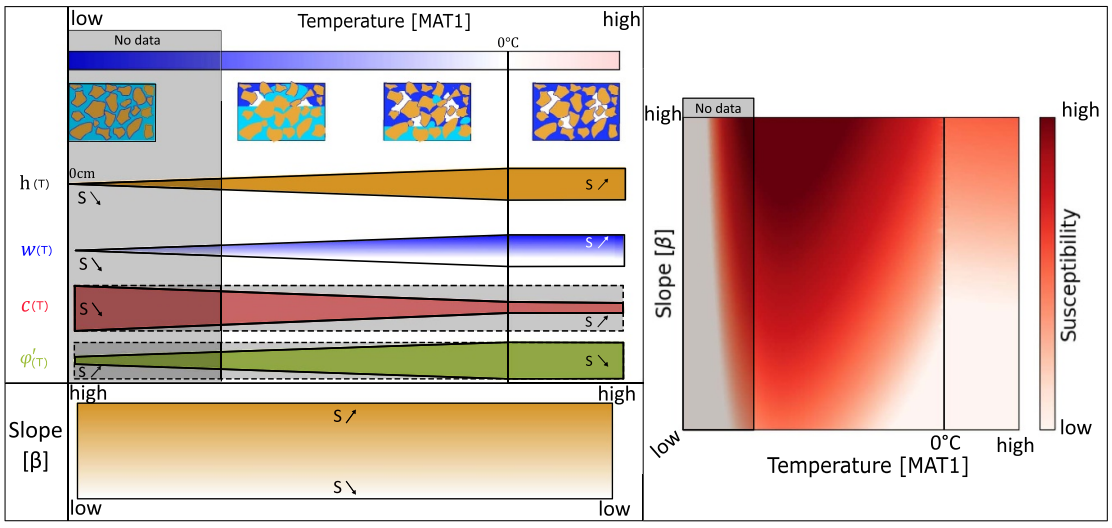

Figure 10. Schematic highlighting the complexity in how properties influencing the susceptibility (*S*) to slope instability change with soil temperature. Shaded dotted areas highlight relatively high uncertainty in defining cohesion and internal friction angle due to temperature variations, water phase change, and material properties.

the cumulative pore pressure induced by the unfrozen water column (figure 2(h)) and the weight of the soil column surpass a critical threshold. In this watershed, we find that the shearing surface is 0.4–0.75 m deep when slopes are larger than 15.5°. These values align with the literature (Lewkowicz and Clarke 1998, Harris *et al* 2011, Bommer *et al* 2012) and notably with Harris and Lewkowicz (2000), who suggested that movements could be initiated on slopes exhibiting a shear surface at a depth of 0.6 m.

The maximum thawing depth and the MAT1 exert control over the observed fluxes. Fluxes exceeding 0.03 m^2 yr^{-1} occur either with MAT1 values of −2.4 °C and below coupled with a shallow shear surface (−0.9 m and shallower), or MAT1 values of −1.65 °C and above associated with a deep shear zone (base at −1.1 m and deeper; supplementary 2).

In addition, two-sided freezing, which is often associated with the plug-like flow solifluction (Matsuoka 2001), is observed across the watershed (figure 5). The formation of ice lenses at the top of permafrost creates a shear zone upon thawing that allows the entire layer to move along this shear zone as a cohesive unit. The depth and the composition of this shearing surface likely control the movement's pattern and extent.

Beyond these shallow processes, the possibility of deep slow creep within the permafrost (Dallimore *et al* 1996, Foriero *et al* 1998), with rates ranging from millimeters to centimeters per year, arouses interest in a multiyear analysis perspective, where cumulative movements may pose potential hazards. Looking at the observed fluxes and at the precision and capacity limitations of our instrumentation and GPS measurements, coupled with the fact that the studied period covers only a single thawing season, we are unable to distinguish the possible presence of such slow movements from the solifluction processes.

Our data show that permafrost table depth, soil temperature, and thaw front progression vary across the studied hillslopes, influencing the timing and locations of hillslope movements. Spatial soil temperature variability across the watershed is a reliable indicator of the spatio-temporal heterogeneity of these movements. The warmest, south facing slope has a substantial movement history indicated by multiple lobes on the surface (supplementary 3, Del Vecchio *et al* (2023)), but is currently experiencing minimal to no movement. The south-east facing slope, with intermediate MAT1, is currently undergoing the most substantial movements. The coldest, east facing slope is displaying movement, although to a lesser degree due to the presence of colder permafrost and shallower thawing depth. This indicates a progressive soil deformation pattern with progressing permafrost thaw, intricately associated with the parabolic susceptibility to slope instability as depicted in figure 10 (right panel). A plausible hypothesis is that deformation rates are decreasing on the south facing slope, since thaw depths are already very deep. In contrast, deformation rates may be peaking on the south-east facing slope, and beginning to accelerate on the east facing slope.

While studies such as those by Kokelj *et al* (2015) or Matsuoka (1996) emphasize a correlation between rainfall and soil movements in permafrost terrain, our findings show that the influence of rainfall on the observed movements is limited, at least during the monitoring period. The locations associated with increase in soil movement following rain events show variable timing after the rain events without clear patterns across the landscape. This is likely due to the fact that soil saturation is high across the watershed, leading to limited infiltration of rainwater, and hence negligible changes in pore water pressures. However, large rainfall events may hasten soil movement via increased heat transfer, accelerated permafrost thaw (Mekonnen *et al* 2021), and increase in porewater pressure.

This study, like other studies (e.g. Kinnard and Lewkowicz 2005, Lewkowicz and Harris 2005, Bommer *et al* 2012), shows that in Arctic environments soil temperature plays a pivotal role in triggering and regulating shallow slope movements. Soil ice content and thawing depth (h) control the critical soil parameters governing slope stability, including pore pressure (u), cohesion (c) and internal friction angle (φ') (figure 10, left panel) and subsequent slope movements (figure 10, right panel). The computed Fs proxy shows that, besides slope angle, the risk of hillslope movements varies strongly as a function of temperature, and that the use of ground temperature may help identify when soil thaw is associated with high susceptibility to slope movements.

6. Conclusion

The results of this study indicate that most of the shallow movements observed across warm permafrost hillslopes occur along the thaw-freeze interface. These soil movements are triggered upon reaching thawing depths between 0.4–0.75 m, after which the entire layer moves cohesively as a unified entity. Notably, this study finds the largest movements in colder areas, which can be attributed to ice-lens formation via two-sided freezing in these locations. Furthermore, the study underscores the complexity of processes involved in slope instability through the estimation of a Fs proxy, underlining the importance of capturing the depth profile of soil temperature, water and ice content, and slope to estimate landscape susceptibility to slope instability. The outcomes of this study exhibit promising potential for predicting slope susceptibility to movement across Arctic regions. A multi-year analysis will provide additional information on trends in thaw depths and their influence on soil movement. Moreover, a more holistic understanding could be obtained by integrating data

from multiple sites that encompass different geological characteristics, exposure to various environmental factors, and diverse slope setups. Overall, this study contributes to our understanding of the main factors controlling slope movements, providing valuable insights for future mitigation strategies, hazard assessment, and estimates of soil carbon stocks and fluxes.

Data availability statement

The data that support the findings of this study are openly available at the following URL/DOI: https://data.ess-dive.lbl.gov/datasets/doi:10.15485/2251663.

Acknowledgments

This research is part of the Next Generation Ecosystem Experiments (NGEE) Arctic project, which has been funded by the Office of Biological and Environmental Research in the DOE Office of Science (Grant DE-AC02-05CH11231).

ORCID iDs

Sylvain Fiolleau https://orcid.org/0000-0001-6269-8676
Ian Shirley https://orcid.org/0000-0002-2229-1414
Chen Wang https://orcid.org/0000-0001-9508-7425

References

Beamish A, Neil A, Wagner I and Scott N A 2014 Short-term impacts of active layer detachments on carbon exchange in a high Arctic ecosystem, Cape Bounty, Nunavut, Canada *Polar Biol.* **37** 1459–68

Bommer C, Fitze P and Schneider H 2012 Thaw-consolidation effects on the stability of alpine talus slopes in permafrost *Permafr. Periglac. Process.* **23** 267–76

Busey B, Bolton B, Wilson C and Cohen L, 2017 Surface Meteorology at Teller Site Stations, Seward Peninsula, Alaska, Ongoing from 2016 *Next Generation Ecosystem Experiments Arctic Data Collection* (Oak Ridge National Laboratory, U.S. Department of Energy) (https://doi.org/10.5440/1437633) (Accessed 6 January 2023)

Dafflon B *et al* 2022 A distributed temperature profiling system for vertically and laterally dense acquisition of soil and snow temperature *The Cryosphere* **16** 719–36

Dallimore S R, Nixon F M, Egginton P A and Bisson J G 1996 Deep-seated creep of massive ground ice, Tuktoyaktuk, NWT, Canada *Permafr. Periglac. Process.* **7** 337–47

Darrow M M, Gyswyt N L, Simpson J M, Daanen R P and Hubbard T D 2016 Frozen debris lobe morphology and movement: an overview of eight dynamic features, southern Brooks Range, Alaska *The Cryosphere* **10** 977–93

Del Vecchio J, Lathrop E R, Dann J B, Andresen C G, Collins A D, Fratkin M M, Zwieback S, Glade R C and Rowland J C 2023 Patterns and rates of soil movement and shallow failures across several small watersheds on the Seward Peninsula, Alaska *Earth Surf. Dyn.* **11** 227–45

Dobricic S, Russo S, Pozzoli L, Wilson J and Vignati E 2020 Increasing occurrence of heat waves in the terrestrial Arctic *Environ. Res. Lett.* **15** 024022

Fiolleau S, Uhlemann S, Wielandt S and Dafflon B 2023 Understanding slow-moving landslide triggering processes using low-cost passive seismic and inclinometer monitoring *J. Appl. Geophys.* **215** 105090

Foriero A, Ladanyi B, Dallimore S R, Egginton P A and Nixon F M 1998 Modelling of deep seated hill slope creep in permafrost *Can. Geotech. J.* **35** 560–78

Fu Y, Jiang Y, Wang J, Liu Z and Lu X 2021 Mechanical properties of frozen glacial tills due to short periods of thawing *Front. Earth Sci.* **9** 799467

Hampton M A and Winters W J 1983 *Geotechnical Framework Study of the Northern Bering Sea, Alaska* (The Survey)

Harris C, Kern-Luetschg M, Christiansen H H and Smith F 2011 The role of interannual climate variability in controlling solifluction processes, Endalen, Svalbard *Permafr. Periglac. Process.* **22** 239–53

Harris C and Lewkowicz A G 2000 An analysis of the stability of thawing slopes, Ellesmere Island, Nunavut, Canada *Can. Geotech. J.* **37** 449–62

Harris C, Smith J S, Davies M C R and Rea B 2008 An investigation of periglacial slope stability in relation to soil properties based on physical modelling in the geotechnical centrifuge *Geomorphology* **93** 437–59

Herman J and Usher W 2017 SALib: an open-source Python library for sensitivity analysis *J. Open Source Softw.* **2** 97

Hjort J, Streletskiy D, Doré G, Wu Q, Bjella K and Luoto M 2022 Impacts of permafrost degradation on infrastructure *Nat. Rev. Earth Environ.* **3** 24–38

Hjort J, Ujanen J, Parviainen M, Tolgensbakk J and Etzelmüller B 2014 Transferability of geomorphological distribution models: evaluation using solifluction features in subarctic and Arctic regions *Geomorphology* **204** 165–76

Huang W, Mao X, Wu Q and Chen L 2022 Experimental study on shear characteristics of the silty clay soil-ice interface *Sci. Rep.* **12** 19687

Iwanaga T, Usher W and Herman J 2022 Toward SALib 2.0: advancing the accessibility and interpretability of global sensitivity analyses *Socio-Environ. Syst. Modelling* **4** 18155

Jaeger J C, Cook N G W and Zimmerman R 2009 *Fundamentals of Rock Mechanics* (Wiley)

Jafarov E E, Coon E T, Harp D R, Wilson C J, Painter S L, Atchley A L and Romanovsky V E 2018 Modeling the role of preferential snow accumulation in through talik development and hillslope groundwater flow in a transitional permafrost landscape *Environ. Res. Lett.* **13** 105006

Kinnard C and Lewkowicz A G 2005 Movement, moisture and thermal conditions at a turf-banked solifluction lobe, Kluane Range, Yukon Territory, Canada *Permafr. Periglac. Process.* **16** 261–75

Kokelj S V, Tunnicliffe J, Lacelle D, Lantz T C, Chin K S and Fraser R 2015 Increased precipitation drives mega slump development and destabilization of ice-rich permafrost terrain, northwestern Canada *Glob. Planet. Change* **129** 56–68

Lader R, Sousanes P, Bhatt U S, Walsh J E and Bieniek P A 2023 Climate Indicators of Landslide Risks on Alaska National Park Road Corridors *Atmosphere* **14** 34

Lafrenière M J and Lamoureux S F 2013 Thermal perturbation and rainfall runoff have greater impact on seasonal solute loads than physical disturbance of the active layer *Permafr. Periglac. Process.* **24** 241–51

Lathrop E, Nutt M, Wilson C, Bolton R, Perkins G and Harris R 2021 *Soil Moisture, Physical and Chemical Properties Coincident with Airborne SAR Data Collections for 2017 and 2019 (Seward Peninsula, Alaska)* (https://doi.org/10.5440/1854940)

Lewkowicz A G and Clarke S, 1998 Late-summer solifluction and active layer depths, Fosheim Peninsula, Ellesmere Island, Canada *Proc. 6th Int. Conf. on Permafrost* (Centre d'études Nordiques, Université Laval) pp 641–66

Lewkowicz A G and Harris C 2005 Frequency and magnitude of active-layer detachment failures in discontinuous and

continuous permafrost, northern Canada *Permafr. Periglac. Process.* **16** 115–30
Lewkowicz A G and Way R G 2019 Extremes of summer climate trigger thousands of thermokarst landslides in a High Arctic environment *Nat. Commun.* **10** 1329
Lipovsky P S, Coates J, Lewkowicz A G and Trochim E 2006 *Active-layer Detachments following the Summer 2004 Forest Fires near Dawson City, Yukon* (*Yukon Exploration and Geology 2005)* ed D S Emond, G D Bradshaw, L L Lewis and L H Weston (Yukon Geological Survey) pp 175–94
Matsuoka N 1996 Soil moisture variability in relation to diurnal frost heaving on Japanese high mountain slopes *Permafr. Periglac. Process.* **7** 139–51
Matsuoka N 2001 Solifluction rates, processes and landforms: a global review *Earth-Sci. Rev.* **55** 107–34
McRoberts E C and Morgenstern N R 1974 The stability of thawing slopes *Can. Geotech. J.* **11** 447–69
Mekonnen Z A, Riley W J, Grant R F and Romanovsky V E 2021 Changes in precipitation and air temperature contribute comparably to permafrost degradation in a warmer climate *Environ. Res. Lett.* **16** 024008
Mithan H T, Hales T C and Cleall P J 2021 Topographic and ground-ice controls on shallow landsliding in thawing Arctic permafrost *Geophys. Res. Lett.* **48** e2020GL092264
Morgenstern N R and Nixon J F 1971 One-dimensional consolidation of thawing soils *Can. Geotech. J.* **8** 558–65
Nater P, Arenson L U and Springman S M, 2008 Choosing geotechnical parameters for slope stability assessments in alpine permafrost soils *Ninth Int. Conf. on Permafrost* (University of Alaska Fairbanks) pp 1261–6
Olefeldt D *et al* 2016 Circumpolar distribution and carbon storage of thermokarst landscapes *Nat. Commun.* **7** 13043
Patton A I, Rathburn S L and Capps D M 2019 Landslide response to climate change in permafrost regions *Geomorphology* **340** 116–28
Pautler B G, Simpson A J, Mcnally D J, Lamoureux S F and Simpson M J 2010 Arctic permafrost active layer detachments stimulate microbial activity and degradation of soil organic matter *Environ. Sci. Technol.* **44** 4076–82
Rowley T, Giardino J R, Granados-Aguilar R and Vitek J D 2015 Periglacial processes and landforms in the critical zone *Developments in Earth Surface Processes* ed J R Giardino and C Houser (Elsevier) ch 13, pp 397–447
Singhania A, 2020 National Center for Airborne Laser Mapping (NCALM) Lidar DEM data from five NGEE Arctic Sites, Seward Peninsula, Alaska, August 2021 (No. NGA270) *Next Generation Ecosystems Experiment* (Arctic, Oak Ridge National Laboratory (ORNL), Oak Ridge, TN (US); NGEE Arctic, Oak Ridge National Laboratory (ORNL)) (https://doi.org/10.5440/1832016)
Smith S L, O'Neill H B, Isaksen K, Noetzli J and Romanovsky V E 2022 The changing thermal state of permafrost *Nat. Rev. Earth Environ.* **3** 10–23
Sobol′ I M 2001 Global sensitivity indices for nonlinear mathematical models and their Monte Carlo estimates *Math. Comput. Simul.* **55** 271–80
Thornton P E, Thornton M M and Vose R S 2016 Daymet: annual tile summary cross-validation statistics for North America *Version 3* (ORNL DAAC) (https://doi.org/10.3334/ORNLDAAC/1348)
Till A B, Dumoulin J A, Werdon M B and Bleick H A 2011 *Bedrock Geologic Map of the Seward Peninsula, Alaska, and Accompanying Conodont Data* (U.S. Department of the Interior U.S. Geological Survey)
Turetsky M R *et al* 2020 Carbon release through abrupt permafrost thaw *Nat. Geosci.* **13** 138–43
Uhlemann S *et al* 2023 Estimating permafrost distribution using co-located temperature and electrical resistivity measurements *Geophys. Res. Lett.* **50** e2023GL103987
Uhlemann S, Dafflon B, Peterson J, Ulrich C, Shirley I, Michail S and Hubbard S S 2021 Geophysical monitoring shows that spatial heterogeneity in thermohydrological dynamics reshapes a transitional permafrost system *Geophys. Res. Lett.* **48** e2020GL091149
Vascik B A, Booth A M, Buma B and Berti M 2021 Estimated amounts and rates of carbon mobilized by landsliding in old-growth temperate forests of SE Alaska *J. Geophys. Res. Biogeosci.* **126** e2021JG006321
Wang T, Jia H, Sun Q and Li G 2022 Effect of the frozen layer on the stability of cut soil slopes during seasonal freezing and thawing *Res. Cold Arid Reg.* **14** 281–92
Washburn A L 1980 *Geocryology: A Survey of Periglacial Processes and Environments* (Wiley)
Wielandt S, Uhlemann S, Fiolleau S and Dafflon B 2022 Low-power, flexible sensor arrays with solderless board-to-board connectors for monitoring soil deformation and temperature *Sensors* **22** 2814
Wielandt S, Uhlemann S, Fiolleau S and Dafflon B 2023 TDD LoRa and delta encoding in low-power networks of environmental sensor arrays for temperature and deformation monitoring *J. Signal Process. Syst.* **95** 831–43